

Antiproton–nucleus quasi-bound states within the 2009 version of the Paris $\bar{N}N$ potential

Jaroslava Hrtánková^{1,*} and Jiří Mareš¹

¹Nuclear Physics Institute, 250 68 Řež, Czech Republic

Abstract. We studied the \bar{p} interactions with the nuclear medium within the 2009 version of the Paris $\bar{N}N$ potential model. We constructed the \bar{p} –nucleus optical potential using the Paris S - and P -wave $\bar{p}N$ scattering amplitudes and treated their strong energy and density dependence self-consistently. We considered a phenomenological P -wave term as well. We calculated \bar{p} binding energies and widths of the \bar{p} bound in various nuclei. The P -wave potential has very small effect on the calculated \bar{p} binding energies, however, it reduces the corresponding widths noticeably. Moreover, the S -wave potential based on the Paris amplitudes supplemented by a phenomenological P -wave term yields the \bar{p} binding energies and widths in very good agreement with those obtained within the RMF model consistent with \bar{p} -atom data.

1 Introduction

The antiproton–nucleus interaction below threshold have been so far studied within phenomenological RMF approaches [1, 2]. The G -parity motivated \bar{p} coupling constants were used to construct the \bar{p} –nucleus potential. The absorption of \bar{p} was accounted for in terms of a purely phenomenological optical potential. The \bar{p} optical potential was confronted with \bar{p} atom data. It was found that the \bar{p} coupling constant have to be properly scaled in order to be consistent with the data. Consequently, the \bar{p} potential was applied in the calculations of \bar{p} quasi-bound states in various nuclei [2].

However, it is desirable to study the \bar{p} interactions with the nuclear medium within other theoretical approaches, such as microscopic models of $\bar{N}N$ interaction based on meson-exchange models [3–5] or chiral $\bar{N}N$ interaction models [6, 7]. Comparison between these $\bar{N}N$ interaction models could bring valuable information about in-medium \bar{p} interactions in the direct confrontation with the data from \bar{p} atoms and \bar{p} scattering off nuclei, as well as predictions for \bar{p} -nuclear quasi-bound states.

Recently, the 2009 version of the Paris $\bar{N}N$ potential [3] was confronted by Friedman *et al.* with the \bar{p} -atom data and antinucleon interactions with nuclei up to 400 MeV/c, including elastic scattering and annihilation cross sections [8]. The analysis revealed the necessity to include the P -wave interaction in order to describe the \bar{p} atom data. The Paris S -wave potential supplemented by a phenomenological P -wave term was found to fit the data on low-density, near-threshold \bar{p} -nucleus interaction. This fact stimulated us to apply it in the present calculations of \bar{p} -nuclear quasi-bound states and explore the effect of the P -wave interaction on \bar{p} binding energies and widths of \bar{p} -nuclear states.

*e-mail: hrtankova@ujf.cas.cz

In Section 2, we briefly introduce the model applied in our calculations. Section 3 presents few representative results together with the discussion of the main findings of our study.

2 Methodology

The binding energies $B_{\bar{p}}$ and widths $\Gamma_{\bar{p}}$ of \bar{p} quasi-bound states in a nucleus are obtained by solving self-consistently the Dirac equation with the optical potential

$$[-i\alpha \cdot \nabla + \beta m_{\bar{p}} + V_{\text{opt}}(r)]\psi_{\bar{p}} = \epsilon_{\bar{p}}\psi_{\bar{p}}, \quad (1)$$

where $m_{\bar{p}}$ is the mass of the antiproton and $\epsilon_{\bar{p}} = -B_{\bar{p}} - i\Gamma_{\bar{p}}/2$ ($B_{\bar{p}} > 0$). The S -wave \bar{p} -nucleus optical potential V_{opt} enters the Dirac equation as the time component of a 4-vector and is constructed in a ‘ $t\rho$ ’ form as follows:

$$2E_{\bar{p}}V_{\text{opt}}(r) = -4\pi \left(F_0 \frac{1}{2}\rho_p(r) + F_1 \left(\frac{1}{2}\rho_p(r) + \rho_n(r) \right) \right). \quad (2)$$

Here, $E_{\bar{p}} = m_{\bar{p}} - B_{\bar{p}}$, F_0 and F_1 are isospin 0 and 1 in-medium amplitudes, and $\rho_p(r)$ [$\rho_n(r)$] is the proton (neutron) density distribution calculated within the RMF NL-SH model [9]. The in-medium amplitudes F_0 and F_1 entering Eq. (2) account for Pauli correlations in the nuclear medium. They are constructed from the free-space $\bar{p}N$ amplitudes using the multiple scattering approach of Wass *et al.* [10] (WRW)

$$F_1 = \frac{\frac{\sqrt{s}}{m_N} f_{\bar{p}n}^S(\sqrt{s})}{1 + \frac{1}{4}\xi_k \frac{\sqrt{s}}{m_N} f_{\bar{p}n}^S(\sqrt{s})\rho(r)}, \quad F_0 = \frac{\frac{\sqrt{s}}{m_N} [2f_{\bar{p}p}^S(\sqrt{s}) - f_{\bar{p}n}^S(\sqrt{s})]}{1 + \frac{1}{4}\xi_k \frac{\sqrt{s}}{m_N} [2f_{\bar{p}p}^S(\sqrt{s}) - f_{\bar{p}n}^S(\sqrt{s})]\rho(r)}. \quad (3)$$

Here, $f_{\bar{p}n}^S$ ($f_{\bar{p}p}^S$) denotes the free-space c.m. $\bar{p}n$ ($\bar{p}p$) S -wave scattering amplitude derived from the Paris $\bar{N}N$ potential as a function of Mandelstam variable \sqrt{s} , m_N represents the mass of the nucleon and $\rho(r) = \rho_p(r) + \rho_n(r)$. The factor \sqrt{s}/m_N transforms the amplitudes from the two-body frame to the \bar{p} -nucleus frame. The Pauli correlation factor ξ_k is defined as follows

$$\xi_k = \frac{9\pi}{k_F^2} \left(4 \int_0^\infty \frac{dr}{r} \exp(ikr) j_1^2(k_F r) \right), \quad (4)$$

where $j_1(k_F r)$ is the spherical Bessel function, k_F is the Fermi momentum and $k = \sqrt{(\epsilon_{\bar{p}} + m_{\bar{p}})^2 - m_{\bar{p}}^2}$ is the antiproton momentum. The integral in Eq.(4) can be solved analytically. The resulting expression is of the form

$$\xi_k = \frac{9\pi}{k_F^2} \left[1 - \frac{q^2}{6} + \frac{q^2}{4} \left(2 + \frac{q^2}{6} \right) \ln \left(1 + \frac{4}{q^2} \right) - \frac{4}{3} q \left(\frac{\pi}{2} - \arctan \left(\frac{q}{2} \right) \right) \right], \quad (5)$$

where $q = -ik/k_F$.

The analysis of \bar{p} atom data [8] revealed that it is necessary to supplement the Paris S -wave potential by the P -wave interaction to make the real \bar{p} potential attractive in the relevant low-density region of a nucleus. To incorporate the P -wave interaction in our model we supplement the r.h.s. of the S -wave optical potential in Eq. (2) [$2E_{\bar{p}}V_{\text{opt}}^S = q(r)$] by a gradient term [8]:

$$2E_{\bar{p}}V_{\text{opt}}(r) = q(r) + 3\nabla \cdot \alpha(r)\nabla. \quad (6)$$

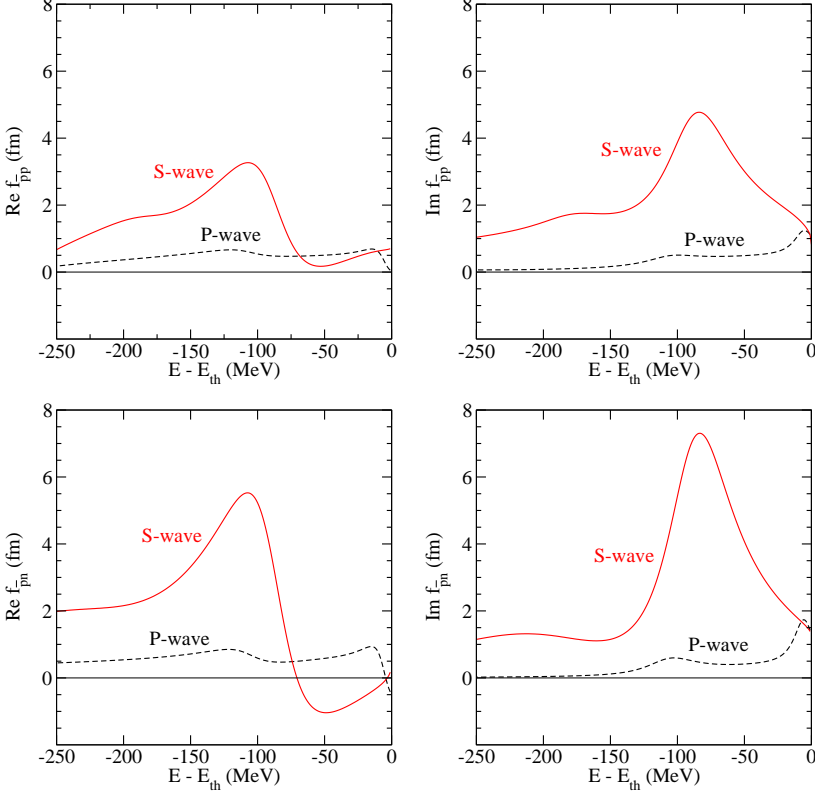


Figure 1. Energy dependence of real (left) and imaginary (right) parts of the Paris 09 $\bar{p}p$ (top) and $\bar{p}n$ (bottom) two-body c.m. scattering amplitudes used in the present calculations: in-medium (Pauli blocked) S -wave amplitudes at $\rho_0 = 0.17 \text{ fm}^{-3}$ and free-space P -wave amplitudes.

The factor $2l + 1 = 3$ in the P -wave part is introduced to match the normalization of the Paris $\bar{N}N$ scattering amplitudes and

$$\alpha(r) = 4\pi \frac{m_N}{\sqrt{s}} \left(f_{\bar{p}p}^P(\sqrt{s}) \rho_p(r) + f_{\bar{p}n}^P(\sqrt{s}) \rho_n(r) \right). \quad (7)$$

Here, $f_{\bar{p}p}^P(\sqrt{s})$ and $f_{\bar{p}n}^P(\sqrt{s})$ represent the Paris P -wave $\bar{p}p$ and $\bar{p}n$ free-space c.m. scattering amplitudes, respectively. We do not consider any medium modifications of the P -wave amplitudes since we assume that the P -wave potential should contribute mainly near the surface of the nucleus due to its gradient form.

The analysis of Ref. [8] also revealed that the optical potential constructed from the Paris S - and P -wave amplitudes fails to reproduce the \bar{p} atom data and that it is mainly due to the P -wave amplitude — its real and imaginary parts had to be scaled by different factors to get reasonable fit. On the contrary, the optical potential based on the Paris S -wave potential supplemented by a purely phenomenological P -wave term with $f_{\bar{p}N}^P = 2.9 + i1.8 \text{ fm}^3$ fits the data well. In our calculations, we adopt both P -wave amplitudes, Paris as well as phenomenological, in order to study their effect on the binding energies and widths of \bar{p} -nuclear states.

The Paris amplitudes used in our calculations are shown in Fig. 1. There are $\bar{p}p$ (top) and $\bar{p}n$ (bottom) medium modified S -wave amplitudes (3) at saturation density $\rho_0 = 0.17 \text{ fm}^{-3}$

and free-space P -wave scattering amplitudes plotted as a function of the energy shift $\delta\sqrt{s} = E - E_{\text{th}}$ with $E_{\text{th}} = m_{\bar{p}} + m_N$. The S -wave amplitudes vary considerably with energy below threshold. The real in-medium $\bar{p}p$ amplitude is attractive in the entire energy region below threshold. The real part of the in-medium $\bar{p}n$ amplitude is attractive for $\delta\sqrt{s} \leq -70$ MeV with a small repulsive dip near threshold. The imaginary parts of the S -wave amplitudes are comparable or even larger than the corresponding real parts. The energy dependence of the free-space P -wave amplitudes is less pronounced than in the S -wave case. Moreover, the P -wave amplitudes are considerably smaller than the in-medium S -wave amplitudes in the region relevant to \bar{p} -nuclear states calculations.

Strong energy dependence of the $\bar{p}N$ amplitudes presented in Fig. 1 requires a proper self-consistent scheme for evaluating the \bar{p} optical potential. The energy argument \sqrt{s} of the amplitudes is expressed in the \bar{p} -nucleus frame where the contributions from antiproton and nucleon kinetic energies are not negligible [11]

$$\sqrt{s} = E_{\text{th}} \left(1 - \frac{2(B_{\bar{p}} + B_{N_{\text{av}}})}{E_{\text{th}}} + \frac{(B_{\bar{p}} + B_{N_{\text{av}}})^2}{E_{\text{th}}^2} - \frac{T_{\bar{p}}}{E_{\text{th}}} - \frac{T_{N_{\text{av}}}}{E_{\text{th}}} \right)^{1/2}. \quad (8)$$

Here, $B_{N_{\text{av}}} = 8.5$ MeV and $T_{N_{\text{av}}}$ are the average binding and kinetic energy per nucleon, respectively, and $T_{\bar{p}}$ represents the \bar{p} kinetic energy. The kinetic energies are evaluated as corresponding expectation values of the kinetic energy operator $\hat{T} = -\frac{\hbar^2}{2m}\Delta$. Since the $B_{\bar{p}}$ appears as an argument in the \sqrt{s} , which in turn serves as an argument for V_{opt} , \sqrt{s} has to be determined self-consistently. Namely, its value obtained by solving Eq. (8) should agree with the value of \sqrt{s} which serves as input in Eq. (3) and thus Eq. (1), as well.

3 Results

We performed self-consistent calculations of \bar{p} -nuclear quasi-bound states in selected nuclei within the model presented in the previous section. We explored the energy and density dependence of the S -wave \bar{p} -nucleus potential as well as the role of the $\bar{p}N$ P -wave interaction, and compared the predictions for \bar{p} binding energies and widths with the phenomenological RMF approach [2].

The $\bar{p}N$ amplitudes are strongly energy and density dependent, as was shown in Fig. 1. Consequently, the depth and shape of the \bar{p} -nucleus potential depend greatly on the energies and densities pertinent to the processes under consideration. It is demonstrated in Fig. 2 where we present the \bar{p} potential in ^{40}Ca calculated for different energies and densities: i) using the Paris free-space S -wave amplitudes at threshold (denoted by ‘th free’), ii) using in-medium Paris S -wave amplitudes at threshold (denoted by ‘th medium’), iii) using in-medium Paris S -wave amplitudes at energies relevant to \bar{p} atoms (constructed following Ref. [8]), and iv) using in-medium Paris S -wave amplitudes at energies relevant to \bar{p} nuclei [\sqrt{s} of Eq. (8)]. The \bar{p} potential constructed using the free-space amplitudes has a repulsive real part and fairly absorptive imaginary part. When the medium modifications of the amplitudes are taken into account, the \bar{p} potential becomes attractive and more absorptive. At the energies relevant to \bar{p} atoms, the \bar{p} potential is more attractive and weakly absorptive. Finally, at the energies relevant to \bar{p} nuclei, the \bar{p} potential is strongly attractive, however, also strongly absorptive. The figure clearly shows that proper self-consistent evaluation of the energy \sqrt{s} is essential.

Next, we performed static and dynamical calculations of \bar{p} binding energies and widths using the Paris $\bar{N}N$ potential. In the static calculations, the core nucleus is not affected by the presence of extra \bar{B} . In the dynamical calculations, the polarization of the nuclear core due to \bar{B} , i.e., changes in the nucleon binding energies and densities, is taken into account. The response of the nuclear core to the extra antiproton is not instant — it could possibly

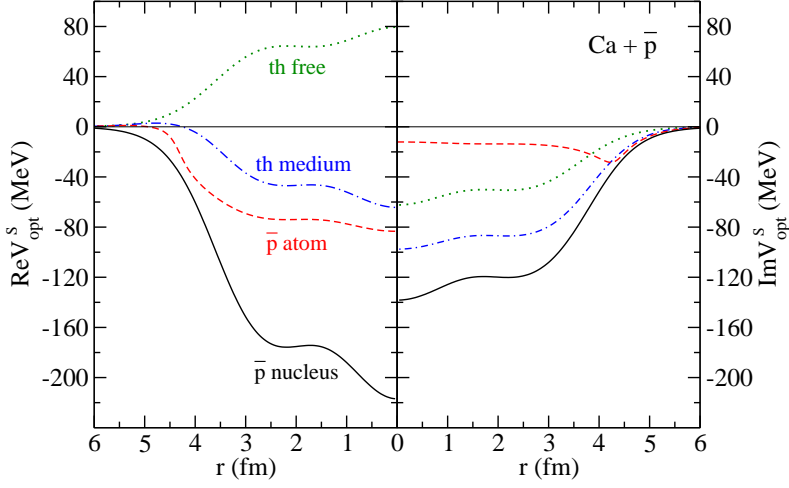


Figure 2. The potential felt by \bar{p} at threshold ('th medium'), in the \bar{p} atom and \bar{p} nucleus, calculated for $^{40}\text{Ca} + \bar{p}$ with in-medium Paris S -wave amplitudes and static RMF densities. The \bar{p} potential calculated using free-space amplitudes at threshold is shown for comparison ('th free').

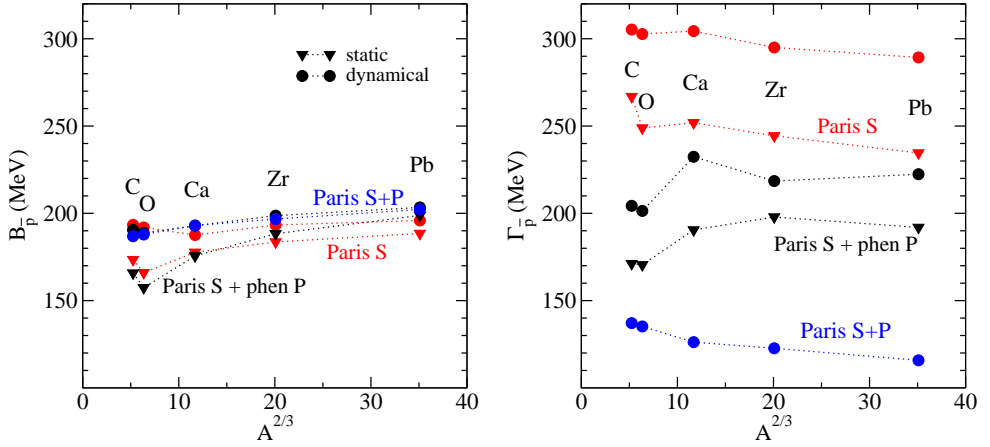


Figure 3. $1s$ \bar{p} binding energies (left panel) and widths (right panel) in various nuclei, calculated statically (triangles) and dynamically (circles) using S -wave Paris potential (red) and including phenomenological P -wave potential (black). The \bar{p} binding energies and widths calculated dynamically using the Paris S + P -wave potential (blue circles) are shown for comparison.

last longer than the lifetime of \bar{p} inside a nucleus [12, 13]. As a result, the antiproton could annihilate before the nuclear core is fully polarized. Our static and dynamical calculations of \bar{p} binding energies and widths may be thus considered as two limiting scenarios.

In Fig. 3, we present $1s$ \bar{p} binding energies (left) and widths (right) as a function of mass number A , calculated statically (triangles) and dynamically (circles) with the Paris S -wave and Paris S -wave + phen. P -wave potentials. We present the \bar{p} binding energies and widths calculated dynamically using the Paris S + P -wave potential for comparison as well.

In dynamical and static calculations alike, the P -wave interaction does not affect much the \bar{p} binding energies — they are comparable with the binding energies evaluated using only the S -wave potential. On the other hand, the \bar{p} widths are reduced significantly when the phenomenological P -wave term is included in the \bar{p} optical potential. The effect is even more pronounced for the Paris P -wave interaction.

The \bar{p} widths calculated dynamically are noticeably larger than the widths calculated statically. It is caused by the increase of the central nuclear density, which exceeds the decrease of the $\bar{p}N$ amplitudes due to the larger energy shift with respect to threshold ($\delta\sqrt{s} \sim -255$ MeV in the dynamical case vs. $\delta\sqrt{s} \sim -200$ MeV in the static case). On the other hand, the \bar{p} binding energies increase only moderately and get closer to each other when the dynamical effects are taken into account. The \bar{p} widths exhibit much large dispersion than the \bar{p} binding energies for the different potentials.

We explored the \bar{p} excited states in selected nuclei as well and compared the results with those obtained within the RMF approach [2]. Fig. 4 shows \bar{p} spectra in ^{40}Ca calculated using the Paris S -wave + phen. P -wave potential and phenomenological RMF approach. The Paris S -wave + phen. P -wave potential yields the $1p$ and $1d$ binding energies slightly larger and thus the s - p and s - d level spacing smaller than the RMF approach. It is an effect of a broader \bar{p} potential well generated by the Paris S -wave + phen. P -wave potential. Nevertheless, both approaches yield comparable \bar{p} widths as well as energies and the overall agreement is surprisingly good.

It is to be noted that there is no spin-orbit splitting of the p and d levels presented in Fig. 4 since the V_{opt} is a central potential constructed from angular momentum-averaged scattering amplitudes. In the RMF approach, the \bar{p} binding energies in $1p$ and $1d$ spin doublets are nearly degenerate, the difference in \bar{p} energies (as well as \bar{p} widths) is up to ~ 1 MeV. This is in agreement with spin symmetry in antinucleon spectra within the RMF approach [14, 15]. In the left panel of Fig. 4 we show the spin-averaged $1p$ and $1d$ \bar{p} binding energies and widths for better comparison with the results obtained with the central Paris potential.

In conclusion, we performed self-consistent calculations of \bar{p} -nuclear quasi-bound states using a microscopic potential, namely the Paris $\bar{N}N$ potential, for the first time. We explored

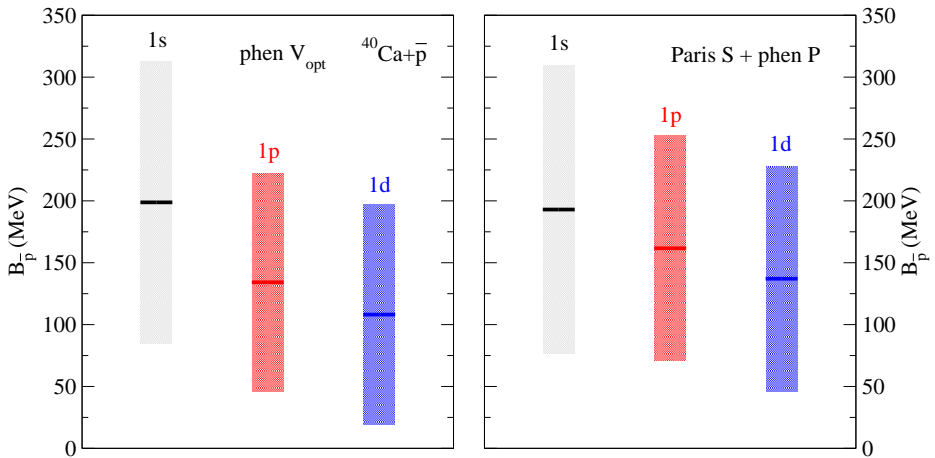


Figure 4. $1s$, $1p$ and $1d$ binding energies (lines) and widths (boxes) of \bar{p} in ^{40}Ca calculated dynamically within the phenomenological RMF \bar{p} optical potential and Paris S -wave + phen. P -wave potential.

the effect of the P -wave interaction on \bar{p} binding energies and widths. We found that the P -wave interaction almost does not affect the binding energies of \bar{p} -nuclear states. This is in sharp contrast to the case of \bar{p} atoms where it was found necessary to include the P -wave interaction in order to increase attraction of the \bar{p} optical potential [8]. Moreover, we found good agreement between the results obtained using the phenomenological RMF potential and the Paris S -wave + phenomenological P -wave potential which are the two potentials consistent with antiprotonic atom data and \bar{p} scattering off nuclei at low energies.

Acknowledgements

We thank E. Friedman and A. Gal for valuable discussions, and B. Loiseau for providing us with the $\bar{N}N$ amplitudes. This work was supported by the GACR Grant No. P203/15/04301S.

References

- [1] T. J. Bürvenich, W. Greiner, I. N. Mishustin, L. M. Satarov, H. Stöcker, Phys. Rev. C **71** (2005) 035201.
- [2] J. Hrtánková, J. Mareš, Nucl. Phys. A **945** (2016) 197.
- [3] B. El-Bennich, M. Lacombe, B. Loiseau, S. Wycech, Phys. Rev. C **79** (2009) 054001.
- [4] T. Hippchen, K. Holinde, W. Plessas, Phys. Rev. C **39** (1989) 761.
- [5] D. Zhou, R. G. E. Timmermans, Phys. Rev. C **86** (2012) 044003.
- [6] K. W. Kang, J. Haidenbauer, U.-G. Meißner, JHEP **1402** (2014) 113.
- [7] L.-Y. Dai, J. Haidenbauer, U.-G. Meißner, JHEP **1707** (2017) 78.
- [8] E. Friedman, A. Gal, B. Loiseau, S. Wycech, Nucl. Phys. A **934** (2015) 101.
- [9] M. M. Sharma, M. A. Nagarajan, P. Ring, Phys. Lett. B **312** (1993) 377.
- [10] T. Wass, M. Rho, W. Weise, Nucl. Phys. A **617** (1997) 449.
- [11] A. Cieplý, E. Friedman, A. Gal, D. Gazda, J. Mareš, Phys. Lett. B **702** (2011) 402.
- [12] A. B. Larionov, I. N. Mishustin, L. M. Satarov, W. Greiner, Phys. Rev. C **78** (2008) 014604.
- [13] A. B. Larionov, I. N. Mishustin, L. M. Satarov, W. Greiner, Phys. Rev. C **82** (2010) 024602.
- [14] J. N. Ginocchio, Phys. Rep. **414** (2005) 165.
- [15] X. T. He, S. G. Zhou, J. Meng, E. G. Zhao, W. Scheid, Eur. Phys. J. A **28** (2006) 265.